Multistage tool path strategy to produce hemispherical shape using single point incremental forming process

Ashish M. Gohil and Bharat A. Modi*

Mechanical Engineering Department,
School of Engineering under Institute of Technology,
Nirma University,
Ahmedabad – 382481, India
Email: ashish.gohil@nirmauni.ac.in
Email: bharat.modi@nirmauni.ac.in
*Corresponding author

Abstract: Single-stage toolpath strategies used in the single point incremental forming process are suffering the problems related to formability, geometric accuracy, and non-uniform thinning. A multistage forming strategy can be used to improve the same, however, it leads to the formation of protrusion defect due to rigid body translation. In this paper, the multistage toolpath strategy has been proposed to circumvent this issue for hemispherical shape which is difficult to produce using a single-stage forming strategy due to 90° tool entry angle at the base. The proposed strategy doesn't require the calculation of rigid body translation and produces the hemispherical shape without the formation of protrusion defect. Enhancement in formability using proposed multistage forming strategy, in terms of depth of forming, uniform strain distribution and thinning have been presented based on experimental and numerical investigation. The limiting value of percentage increase in surface area during the stage is found to be 30.

Keywords: ISF; incremental sheet forming; SPIF; single point incremental forming; multistage tool path; thinning band; strain distribution; rigid body translation; protrusion defect.

Reference to this paper should be made as follows: Gohil, A.M. and Modi, B.A. (2021) 'Multistage tool path strategy to produce hemispherical shape using single point incremental forming process', *Int. J. Mechatronics and Manufacturing Systems*, Vol. 14, Nos. 3/4, pp.181–201.

Biographical notes: Ashish M. Gohil is an Assistant Professor at the Mechanical Engineering Department, Nirma University. His research interests include sheet metal forming and computer-aided manufacturing. He is the author of a number of research studies published at national journals, conference proceedings as well as book chapters.

Bharat A. Modi received his PhD in Engineering at the Indian Institute of Technology, Delhi. He is a Professor at the Department of mechanical engineering, Nirma University. His research interests are related to sheet metal

forming and unconventional machining. He has published research papers at national and international journals, conference proceedings as well as chapters of books.

1 Introduction

Incremental sheet forming (ISF) is a recent process in sheet metal forming industry to produce components in a single piece or batch production which is suitable for customised parts or prototypes. This process is generally performed on a vertical machining centre (VMC). The VMC machine moves the hemispherical ended tool along the predefined tool path using the part program. The tool path is designed in such a way that it forms the component to the size and shape of the finished geometry of the sheet metal component. As the development time in the ISF process is very short, the process is gaining importance as rapid prototyping process for sheet metal component at a low cost. A detail literature review on incremental sheet forming have been provided in the recent paper by Li et al. (2017) throwing insight into the deformation mechanics, process formability, modelling methods and performance measures. The process is having mainly two variants: 1. Single point incremental forming (SPIF), and 2. Two point incremental forming (TPIF). Marked interest in the ISF process is developed in the research community because of the high formability achieved in the process due to local deformation under plane strain mode. Jackson and Allwood (2009) attributed this improved formability to stretching and shear perpendicular to tool direction and shear in tool direction. Process is also having the advantage from the tooling points of view as it needs only hemispherical ended tool which is universal to all the components being manufactured. The process is used by the researchers to produce components related to automobile (Attanasio et al. (2008)) and medical application. Fiorentino et al. (2012) used the ISF process to produce and check the biocompatibility of a prosthesis made from Titanium material. However, its acceptance in industries as the production process is still a problem because of the poor geometric accuracy, poor surface finish and longer time required to manufacture a component.

Different approaches have been adopted by various researchers to overcome the limitations of the process. Among the different process parameters which govern the process, the wall angle of tested geometry and tool path are two of the factors affecting geometric accuracy, surface finish and thinning. Giraldo-Castrillon et al. (2019) through design of experiments concept found that the wall angle is the most significant parameter affecting the deformation process in the SPIF and the TPIF process. Bouhamed et al. (2019b) have implemented the representative volume element and Mori-Takan model in numerical simulation using ABACUS software and found that increase in cone wall angle leads to reduction in the thickness and hence formation of crack. Components can be formed using single-stage or multistage tool path strategy. Tool path can be generated with constant step-depth, variable step-depth or helical tool path strategies. Usually the tool path is generated by slicing the shape in Z-direction using a constant step-depth. Dai et al. (2000) suggested that a tool path should be such that, maximum deformation occurs in less stiff area (centre) and minimum deformation occurs in the high stiff area (periphery) to

obtain a more uniform thinning and to avoid cracking along the periphery. Attanasio et al. (2006) used variable step-depth toolpath as against the conventional constant step-depth tool path in TPIF process with full die support and reported an improvement in geometric accuracy of formed component. Attanasio et al. (2008) have also reported positive results of variable step-depth tool path while producing automotive component having contour shape at the bottom by TPIF process. However, the tool path is reported to take a longer time to manufacture the component. Malhotra et al. (2010) have proposed an automatic 3D tool path generation methodology by using a modified adaptive slicing algorithm. Volumetric error and scallop height were used to quantify and control the geometric accuracy and surface finish of the formed component. Lu et al. (2013) have proposed feature based tool path using equipotential line principle and reported improvement in surface quality, wall thickness and dimensional accuracy on shapes with double bottom geometry, non-axisymmetric cone, and car fender. Bouhamed et al. (2019a) have presented non-associated flow rule model to predict the thickness distribution using ABACUS software. Based on the different approaches discussed above, three approaches have been used in the proposed multistage tool path strategy:

- maximum deformation should be near the centre than towards the periphery to avoid early fracture of component
- variable step-depth to form the hemisphere, i.e., less contours near the base and more contours near the pole region
- Z-depth slicing approach to generate the tool path.

Multistage tool path strategy can also be used to address the issues of geometrical accuracy and non-uniform thinning. It is used mainly to produce high wall angled shapes where single-stage strategy fails to produce the sound components. Bambach et al. (2009) suggested multistage toolpath strategy as an alternative to overbending strategy to limit the springback and improve the geometric accuracy. Kim and Yang (2000) proposed a double-pass forming method in which intermediate pass was obtained based on the predicted thickness strain assuming that deformation occurs only because of shear deformation. More uniform thickness distribution was obtained for ellipsoidal cup and clover cup formed by the double pass strategy than single pass strategy. Duflou et al. (2008) formed cylindrical wall successfully using five-pass multistage tool path with constant wall angle increment strategy. In the study, it was observed that material gets shifted from the bottom to wall region which generally remains undeformed in single stage strategy. Manco et al. (2011) compared four different tool path strategies from the thickness distribution point of view. Decremental slope strategy has given 40% improvement in minimum thickness over a single slope strategy. However, Incremental slope and decremental slope strategies were not effective due to development of protrusion defect as a result of rigid body translation. Liu et al. (2014) proposed two different multistage tool path strategies, M1 (Global average thickness strain) and M2 (Local weighted average thickness strain), based on predicted thickness strains to form the component in TPIF process. Formability using strategy M2 is found to be increased as additional material around the final part region is used in the forming process. Automated tool path generation module is also proposed by Behera et al. (2014) which uses graph topological framework. It was made possible to manufacture a human face mask with improved geometric accuracy using the tool path generated with

this module. Adams et al. (2015) used a cut-and-loft method using computer-aided design (CAD) software to generate intermediate stages. The patient fitted component was prepared successfully by generating the head geometry using a 3-dimensional scanner to obtain the point cloud.

Multistage toolpath strategy is also used in hole-flanging process using the SPIF process. Cui et al. (2010) compared three different multistage toolpath strategy while forming hole flanging using ISF process: Constant increase in diameter, the constant increase in wall angle and combined strategy. The constant increase in diameter strategy was found to give the highest limiting forming ratio (LFR) because it was capable to eliminate the thinning band in the wall. Centeno et al. (2012) used a multistage tool path with constant angle increment and the formability could be improved which was attributed to suppression of necking before fracture.

However, the problem with multistage tool path strategy is that it leads to the formation of the stepped feature (protrusion) at the bottom due to rigid body translation accumulated during the intermediate stages. Malhotra et al. (2011) have proposed a multistage tool path strategy using combined in-to-out and out-to-in tool path to form intermediate stages to predict the rigid body translation which eliminated stepped feature in the base. However, the drawback of the method was that it requires time-consuming FE simulation every time there is a change in material type and thickness of the sheet metal blank. Hence, the work was extended by Xu et al. (2012) by relating stepped feature generation with yield stress and thickness of the material. Accumulative Double Side Incremental Forming strategy (ADSIF) was also proposed by Malhotra et al. (2012) in which rigid body translation was used as an advantage by using the pure in-to-out motion of the tool and better accuracy compared to SPIF and out-to-in DSIF tool path. Smith et al. (2013) studied the deformation mechanics of ADSIF by performing FE analysis and attributed deformation to the bending-unbending of the sheet and squeezing between the tools. ADSIF process also experiences greater through-thickness shear, hydrostatic pressure, and strain as compared to the SPIF process.

The current practice to eliminate the protrusion defect in multistage forming requires cumbersome calculation of the rigid body translation amount and modification of the toolpath to incorporate the same. However, the multistage toolpath strategy proposed in the paper eliminate the formation of stepped feature (protrusion) at the bottom without making any calculation of rigid body translation and subsequent modification of toolpath. In multistage tool path strategy, design of intermediate stages is the most important aspect. In this paper, the multistage tool path strategy has been proposed to design intermediate stages to form hemispherical shape which is difficult to produce in a single-stage using SPIF process as the tool entry angle is 90° from the base and it gradually reduces to 0° at the pole. The proposed strategy also helps in redistribution of material flow and thus helps in achieving more uniform thickness distribution. FE simulation provides valuable information about the behaviour of the process and hence it is carried out using LS-DYNA solver and details of numerical analysis of the result is also presented.

2 Multi-stage tool path strategy for hemispherical shape

In the ISF process, one of the important parameters is the tool path along which the tool is moved by vertical machining centre (VMC) machine to impose local deformation. In this

section, the proposed multistage tool path strategy to form hemispherical shape is discussed in detail.

Following rules have been followed to design the tool path for the intermediate stage for hemispherical shape which can be followed to generate other shapes as well:

1 The intermediate shape should follow the same geometrical shape as final geometrical shape (with larger curvature). This helps in reducing the tool entry angle and helps in shifting the forming towards the pole region which helps in improving the formability.

2 Depth of forming in each successive stage should be equal (total depth divided by the number of stages). This will help in eliminating the generation of stepped feature at the bottom.

Considering the above-mentioned rules for a two-stage forming, first stage is formed to a depth of $H/2$ and radius of first stage as $SR1$. The second stage is formed to a depth of H and radius of SR as shown in Figure 1. A similar strategy can be used for three-stage, four-stage or any number of stages. This strategy leads to a reduction in entry wall angle. With single stage strategy, tool entry angle is 90° for hemispherical shape and with two-stage strategy tool entry angle reduces to 53.13° in the first stage. However, it is important to calculate the radius and centre point of hemisphere during the intermediate stage and finally tool centre points for all the stages.

Figure 1 Intermediate stages to form hemispherical shape

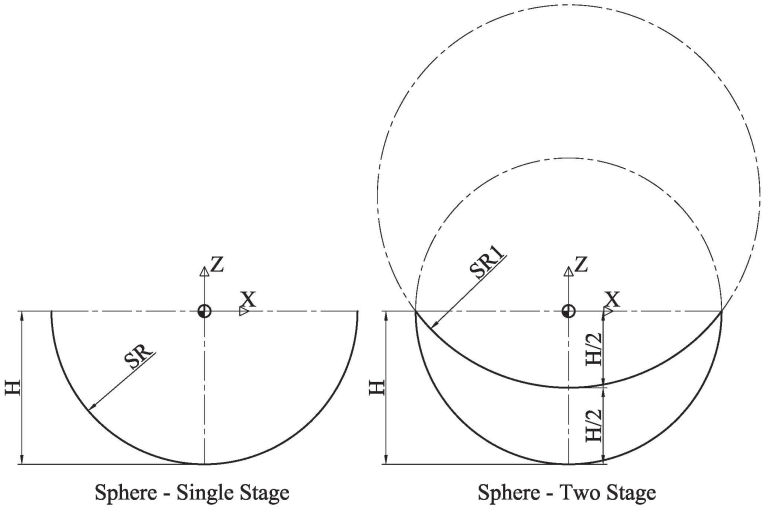

These parameters have been worked out using mathematical formulation as per the following calculations (Refer Figure 2):

Location of the Point A (X_1, Z_1) and Point C(X_3, Z_3) can be obtained from the known radius of the hemisphere SR.

Location of the Point B (X_2, Z_2) can be obtained from the known height of the intermediate stage, i.e., $H/2$ in the case of two-stage forming.

Line L passes through points A & B and line R passes through points C & B.

Slope of line L : $m_L = (Z_2 - Z_1)/(X_2 - X_1)$

Slope of line R : $m_R = (Z_3 - Z_2)/(X_3 - X_2)$

Equation of line L: $Z = m_L(X - X_1) + Z_1$

Equation of line R: $Z = m_R(X - X_2) + Z_2$

Coordinates of midpoint P: $(X_1 + X_2)/2, (Z_1 + Z_2)/2$

Coordinates of midpoint Q: $(X_2 + X_3)/2, (Z_2 + Z_3)/2$

Slope of line OP: $m_P = -1/m_L$

Slope of line OQ: $m_Q = -1/m_R$

Equation of line OP: $Z = m_P[X - (X_1 + X_2)/2] + (Z_1 + Z_2)/2$

Equation of line OQ: $Z = m_Q[X - (X_2 + X_3)/2] + (Z_2 + Z_3)/2$

Coordinates of point O: X, Z

Radius of circle in first stage SR_1 = $\sqrt{(X - X_1)^2 + (Z - Z_1)^2}$

Figure 2 Radius calculation for intermediate hemispheral shape

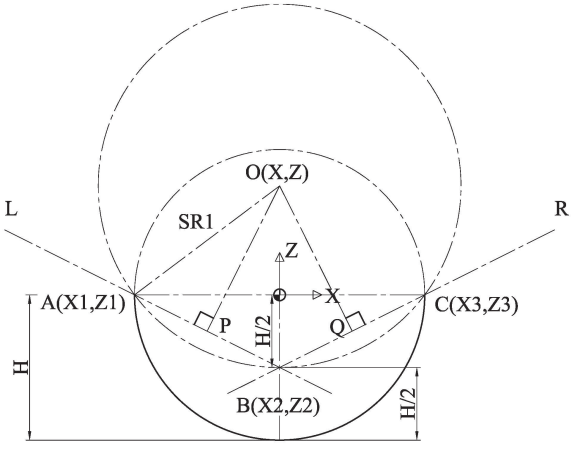

Mathematical formulation to obtain the starting angle at which forming should start in a particular stage, the radius of forming and Z-depth in a stage is given below (Refer Figure 3):

Let TR be the radius of the tool.

From ΔOST, Start angle in a stage: $\phi = \tan^{-1}(ST/OT)$

Forming radius: $r = (SR - TR)\sin(\phi)$

Z-position of tool: $Z = OV - (SR - TR)\cos(\phi) - TR$

Figure 3 Tool position calculation during stages

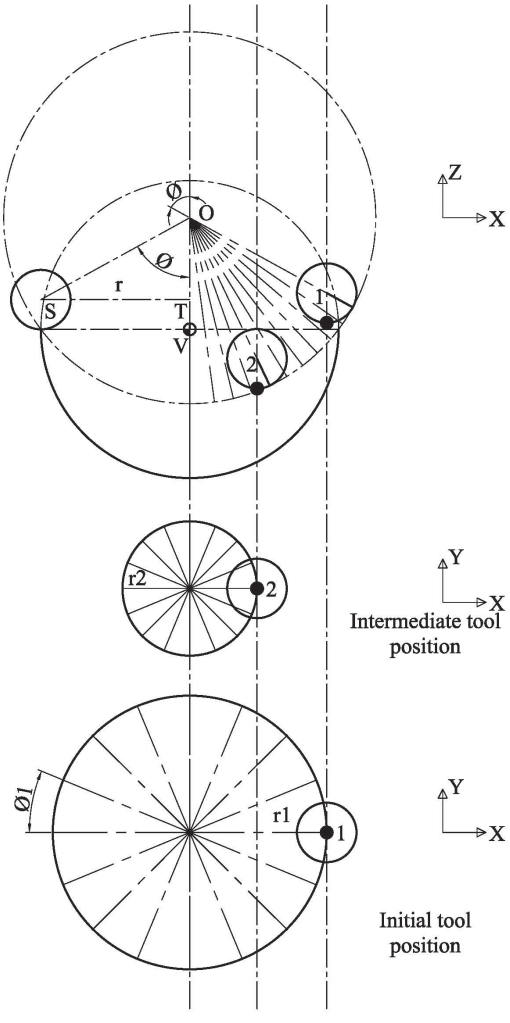

Forming radius and Z-position is used to generate the NC part program for tool movement to generate the hemisphere. However, for FE simulation, time vs. position data is required to move the tool. Hence, the forming radius circle is divided into 360 parts to obtain 360 data points for FE analysis which can be obtained by using following equations:

X-position of tool: $X = r\cos(\phi 1)$

Y-position of tool: $Y = r\sin(\phi 1)$

A software (using Excel VBA) has been developed to generate the NC part program and time vs. position (X, Y and Z) data required for FE analysis. The software incorporates the proposed multistage tool path strategy. Implementation of strategy discussed above is represented through flowchart as shown in Figure 4. Similar steps have been followed to generate time vs. position file required as an input for defining the motion of tool in FE analysis using LS-DYNA.

Figure 4 Flow chart adopted to generate NC part program

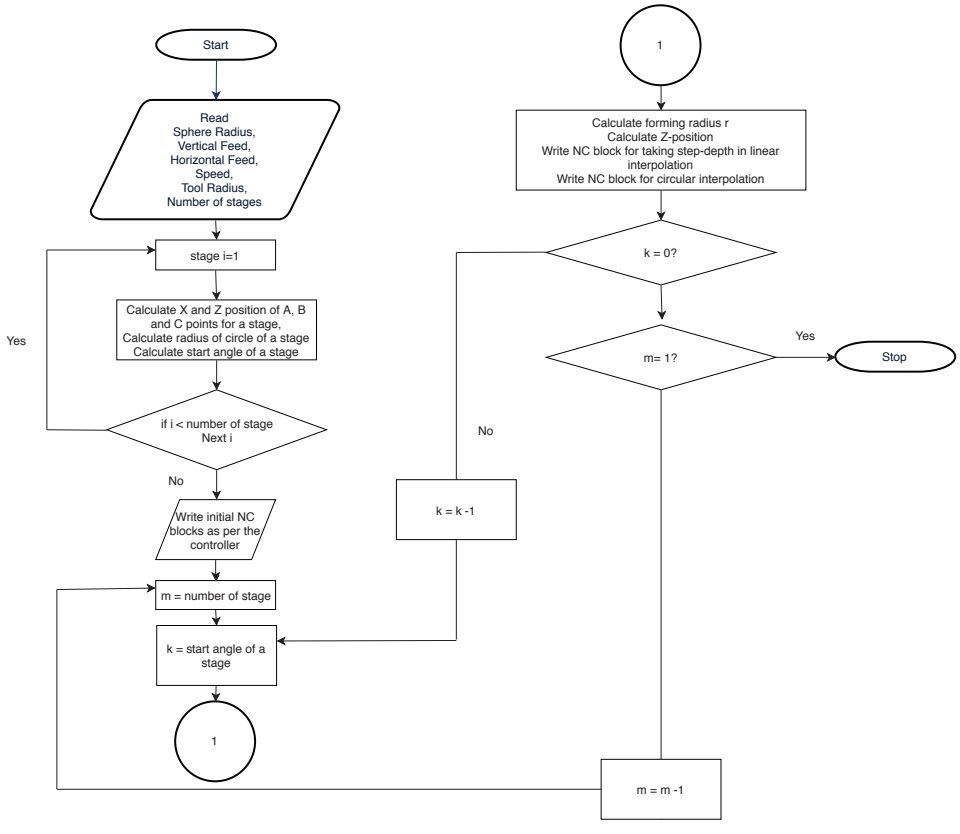

3 Experimental set-up and procedure

Experimental set-up for the present work consists of two main elements: equipment and fixture to clamp the workpiece. Three-axis vertical machining centre (VMC) is used to give the desired motion to the tool. NC part program as discussed in Section 2 is used for generating the hemispherical shape. Schematic representation of the fixture is shown in Figure 5(a) and actual fixture is shown in Figure 5(b). The fixture consists of a backing plate having a cutout of 60 mm diameter to produce hemispherical shape. It is prepared to produce hemisphere of 29 mm radius keeping 1 mm for clearance. Size of the hemisphere and cutout is selected to minimise the bending error near the periphery. The clamping plate is also provided to clamp the sheet metal blank rigidly during forming. Clamping is achieved by using nuts and bolts.

The tool used in the process is having a hemispherical end of 5 mm radius. For tool and fixture, high carbon steel (EN31) material have been used. To improve the surface finish, machine oil is used as a lubricant on the contacting surface during the forming which reduces the friction between the tool and sheet metal blank.

Square sheet metal blanks of AA1100 aluminium material (110 mm ×110 mm) have been used. The thickness of the sheet is 0.71 mm. Chemical composition (Table 1) and mechanical properties (Table 2) of the same have been obtained by performing a spectrometry test and tensile test respectively in a standard testing laboratory.

Figure 5 Fixture to produce hemispherical shape: (a) schematic representation and (b) actual fixture (see online version for colours)

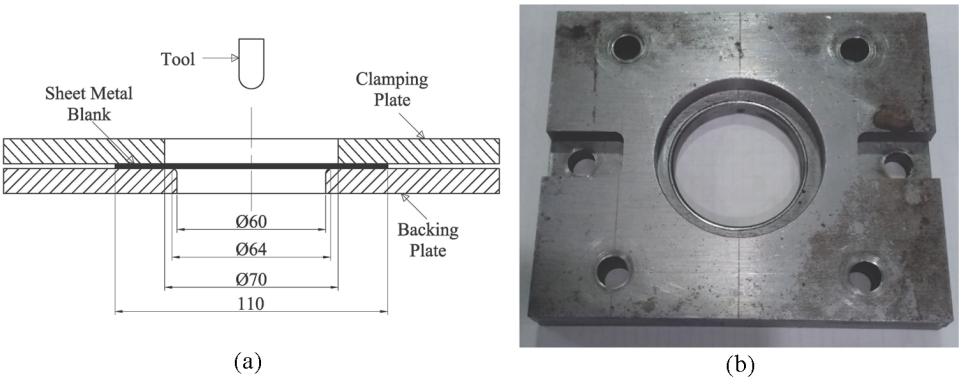

Table 1 Chemical composition of AA1100 aluminium sheet (wt%)

Composition	*Si*	*Fe*	*Mn*	*Zn*	*Ti*	*Ni*	*Pb*	*Al*
Actual	0.1	0.28	0.003	0.005	0.022	0.004	0.001	99.57

Table 2 Mechanical properties of AA1100 aluminium sheet

Parameter	*Symbol*	*Value*	*Unit*
Thickness	t	0.71	mm
Ultimate tensile strength	σ_u	122.88	MPa
Yield strength	σ_y	111.58	MPa
Modulus of elasticity	E	70	GPa
Strength coefficient	K	278.8	MPa
Strain hardening exponent	n	0.2655	
Elongation in 50 mm gauge length	EL	6.16	%

Experiments were performed on the sheet metal blank with engraving for performing circle grid analysis. Circles of 1 mm diameter were engraved on the sheet metal blank by using the laser engraving technique. To ensure that the engraving has no effect on the formability experiments were replicated under same conditions on non-engraved sheet of same material for all the hemisperical component. Variable step-depth strategy have been used to form the hemispherical shape. Step-depth varies from 0.51 mm at base to the 0.01 mm to the pole. All the experiments were conducted with spindle in free condition without any rotational speed. Forming feed of 500 mm/min was kept constant during the experiments.

4 Finite element modelling

In this work, numerical simulations are done with the LS-DYNA solver using the keywords given in LSTC (2015) manual, some of the important one are discussed in this section. The full model is idealised using Belytschko-Tsay shell (BT shell) element formulation which is widely accepted for metal forming simulation (Figure 6). Sheet metal blank is considered as thin shell and its section properties are defined using SECTION_SHELL keyword with 5 integration points. The discretisation of the sheet metal blank is done using an element size of 0.5 mm. The total element count of the sheet metal blank is 10015 and the node count is 10125. Sheet metal blank is modelled with the power law plasticity model with K and n values tabulated in Table 2. Tool is defined as a rigid body. Properties of the same are defined using the material model MAT_RIGID. The backing plate is also modelled as a rigid body. To simplify the model the sheet metal blank size is taken same as the cut-out in the backing plate. The blank is constrained along the periphery. Hence, clamping plate is eliminated in the FE model. The contact between the Sheet metal blank and tool is defined by surface to surface contact method (CONTACT_FORMING_ONE_WAY_ SURFACE_TO_SURFACE) with a coefficient of friction of 0.125. The material behaviour is modelled using power law plasticity material model (MAT_POWER_LAW_PLASTICITY). Rigid body motion is imparted to the tool using BOUNDARY_PRESCRIBED_MOTION_RIGID keyword. Time vs. position (X, Y, and Z) data obtained by Excel VBA program is defined using the DEFINE_CURVE keyword.

Figure 6 Idealised numerical model of ISF process to form hemispherical shape (see online version for colours)

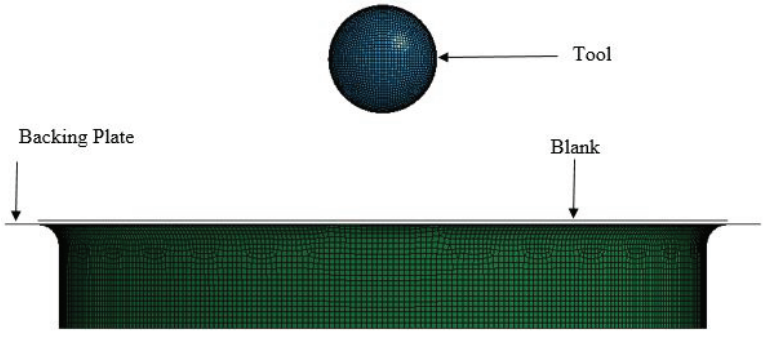

5 Results and discussion

Experiments and FE simulation have been performed as per the experimental procedure given in Section 3. The hemispherical components formed using multistage forming strategy are shown in Figure 7. To understand the multistage forming behaviour of hemispherical shape; depth of forming, area strain analysis, strain distribution, geometric accuracy, and thinning have been considered as the formability indicator and discussed in the following subsections.

Figure 7 Components formed using proposed multistage strategy: (a) single stage, (b) two stage, (c) three stage and (d) four stage (see online version for colours)

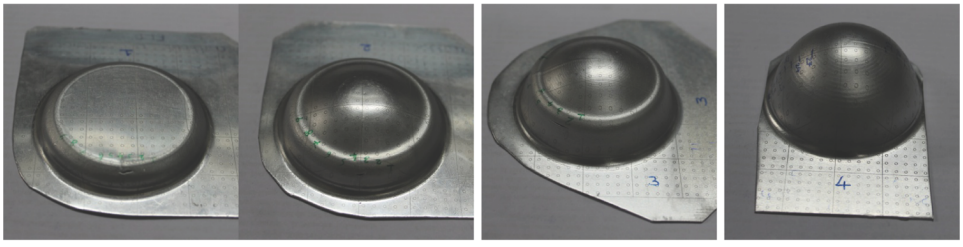

(a) (b) (c) (d)

5.1 Depth of forming

All the experiments have been performed till fracture is visible on the components. During each experiment, depth at the pole is measured from the base using vernier caliper having a least count of 0.02 mm. Results of the depth of forming for the components and FE simulation have been reported in Table 3. In single-stage strategy component failed at the depth of 8.62 mm. In two- and three-stage strategy the components failed at the depth of 17.66 mm and 23.42 mm respectively. However, the component could be formed successfully to the depth of 14.50 mm and 19.34 in the intermediate stages in a two-stage and three-stage forming strategy respectively. The component could be formed successfully to the full depth $H = 29$ mm in four-stage strategy. It shows that with an increase in the number of stages formability is improved. The reason behind the improvement in formability is that in single-stage as angle of entry is 90°, forming is performed in the stiff area near the periphery (clamped region) and hence component fails early which is discussed in detail in Section 5.2.2. However, in a two-, three-, and four-stage strategy gradually more and more material is deformed in the less stiff region towards the pole and less material is deformed along the clamped region due to reduction in angle of entry. Depth of forming achieved in FE simulation is in close agreement with the experimental results. It is evident from the Figure 8 that as the number of stages increases, the deformation initially occurs in biaxial mode and later in plane strain mode, which helps to improve formability.

Table 3 comparison of forming depth (stagewise) obtained experimentally and by FE simulation

	Experimental				*FE simulation*			
	1st stage	*2nd stage*	*3rd stage*	*4th stage*	*1st stage*	*2nd stage*	*3rd stage*	*4th stage*
Strategy	mm	mm	mm	mm	mm	mm	mm	mm
Single stage	8.62	–	–	–	8.34	–	–	–
Two stage	14.5	17.66	–	–	14.5	16.82	–	–
Three stage	9.66	19.34	23.42	–	9.66	19.34	20.6	–
Four stage	7.26	14.5	21.76	28.98	7.26	14.5	21.76	29.288

Depth of the intermediate stage are theoretical.

Figure 8 Strain distribution in the component formed using multistage strategy, superimposed on strain path of the key elements: (a) single stage, (b) two stage, (c) three stage and (d) four stage (see online version for colours)

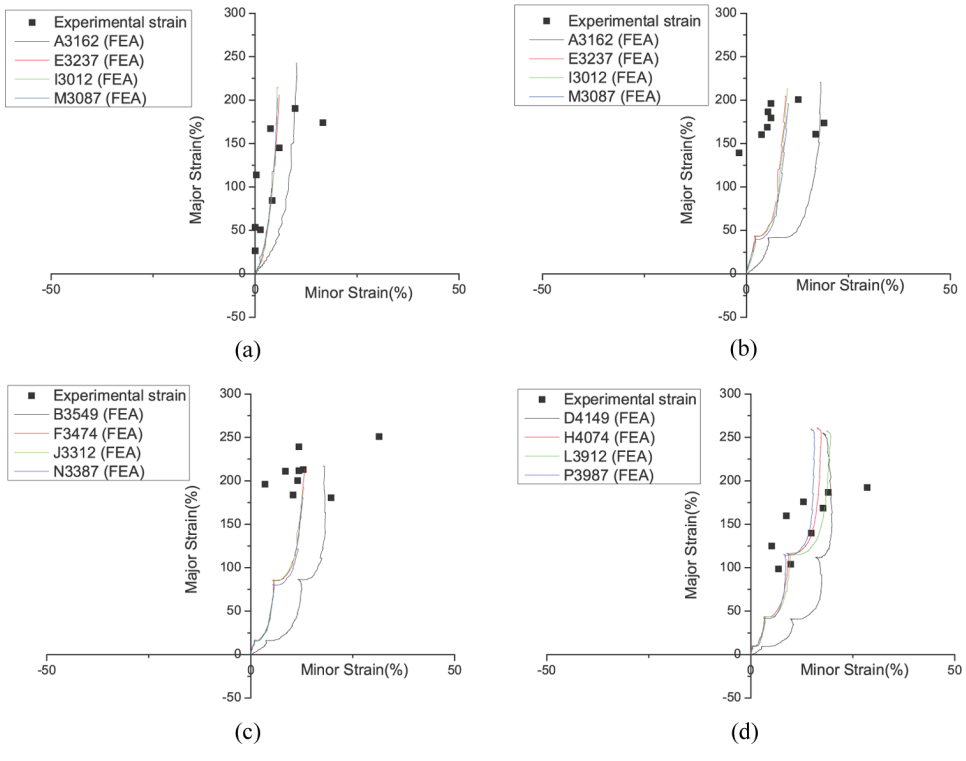

5.2 *Analysis of strain*

Surface area strain analysis

In this section, strain analysis based on surface area calculation is presented (Figure 9). The initial area of the circular blank of radius $SR = 29$ is 2640.74 $\text{mm}^2 (A_i = \pi \times SR^2)$. In single-stage strategy, it is attempted to convert initial circular blank into final hemispherical shell, the surface area of which is 5281.48 $\text{mm}^2 (A_f = 2 \times \pi \times SR \times h)$. Where h is the depth of forming at any stage. For single stage strategy $h = SR$. Hence, in a single-stage forming surface area is increased by 100%. The corresponding surface area strain is calculated to be 0.69 $(\ln(A_f/A_i))$. Higher strain value leads to the failure of the component in single-stage strategy. Similar results have been obtained for a two-, three- and four-stage strategy and presented in Table 4. In a two-stage strategy, % increase in area during the first-stage is 25% with a corresponding increase in strain of 0.22. Lower strain experienced by the component leads to the successful forming of the first stage. However, in the second-stage % increase in area is 60% with a corresponding strain of 0.47, which leads to the failure of the component. From the results of surface area strain (Table 4), it can be seen that the maximum successful % increase in surface area is 30% with a corresponding strain of 0.26. Hence, for the successful forming of a component in multistage strategy increase in the surface area should be restricted to 30%.

Figure 9 Schematics of hemispheres in various stages

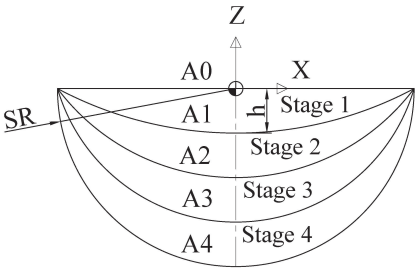

Table 4 Strain in hemispherical component (stagewise) calculated based on surface area

Strategy	*Stage*	*Condition*	*True strain*	*% Increase in area*	*Total strain*
Single stage	1st	Failure	0.69	100.00	
Two stage	1st	Success	0.22	25.00	0.22
	2nd	Failure	0.47	60.00	
Three stage	1st	Success	0.11	11.11	
	2nd	Success	0.26	30.00	0.37
	3rd	Failure	0.33	38.46	
Four stage	1st	Success	0.06	6.25	
	2nd	Success	0.16	17.65	
	3rd	Success	0.22	25.00	
	4th	Success	0.25	28.00	0.69

Strain distribution and strain path

Circle grid analysis is performed by measuring the major and minor dimensions of the deformed grid by using a digital USB microscope. Strain distribution for all four components have been presented in Figure 8 alongwith the strain path obtained through FE simulation. Maximum safe major strain observed during the forming of all the components is of the order of 250%. In single-, two- and three-stage strategy, components have failed in the thinning band (Figure 10).

Figure 10 Cut section of hemisphere in FE simulation of four stage forming strategy (see online version for colours)

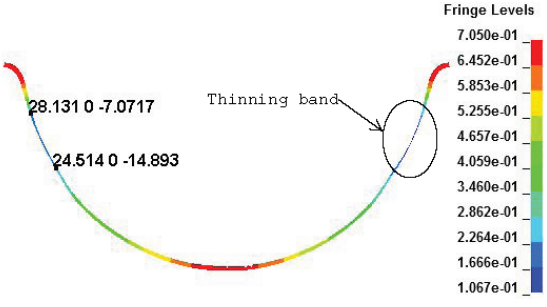

Four consecutive elements (A3162, B3549, C3762, D4149) located at position 1 (0°) as shown in Figure 11 were selected to understand the strain history. The position of the tool where it takes the step-depth is considered as 0° position. Similar points were selected at position 2 (E3237, F3474, G3837, H4074), position 3 (I3012, J3312, K3612, L3912) and position 4 (M3087, N3387, O3687, P3987) at 90°, 180° and 270° respectively. Strain paths obtained for all the components using FE simulation are shown in Figure 8. It is observed that all the elements initially experience circumferential and bi-axial strain and soon deform under plane strain mode. Elements at position 1 (0°) observe severe strain as compared to other positions and exhibit failure. It is noticed that step-depth is given at position 1. Morever, the steps in strainpath indicate the number of stages. In every stage the element first experience strain along circumference then biaxial and major deformation under plane strain mode. As number of stages increases the circumferential strain increases and hence leads to lower thinning before failure. It is also observed that as the number of stages increases element located towards the pole deforms the maximum. In single-stage forming, element A3162 deforms maximum whereas in four-stage strategy element D4149 deforms to the maximum. It gives an indication that the thinning band is shifted towards the pole and hence higher forming is achieved as the numbers of stages are increased.

Figure 11 Location of elements for strain analysis

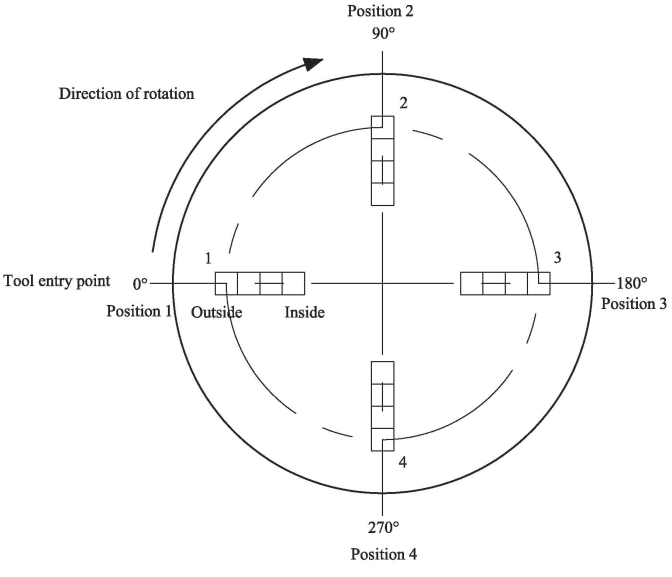

Meridional and circumferential strain

In order to evaluate the development of strain during the multistage forming, one of the highly strained elements located at position 1 (A4149) is chosen. Figure 12 shows the evolution of meridional, circumferential and thickness strain results from the FE simulation of formed hemisphere using four-stage forming strategy. It can be seen that meridional strain increases greatly during the formation of the intermediate stage. The reason for the higher meridional strain is that as the tool passes the thinning band deformation is restricted to the thinning band only as is also evident from the vertical strain path discussed

in previous section. However, the circumferential strain remains very small. Compared to circumferential strain, thickness strain is having a larger value in absolute terms. It indicates that the increase in meridional strain is at the cost of thickness strain. Hence, in the ISF process, the thinning band is observed.

Figure 12 Strain path from FE simulation of forming hemisphere using four stage strategy for element A4149 (see online version for colours)

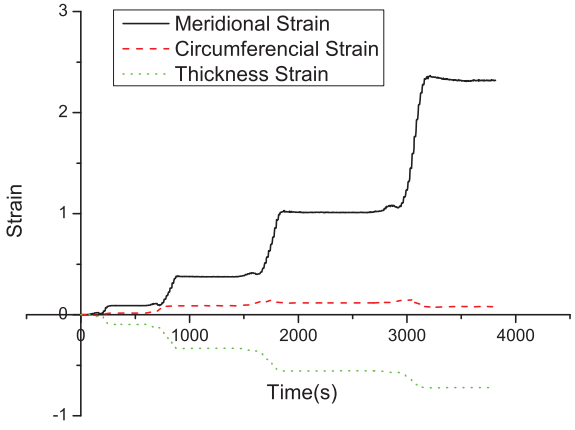

5.2.1 Dimensional accuracy

Dimensional accuracy of the hemispherical shape was measured by using the electronic edge finder of 10 mm diameter using VMC machine. After forming the hemispherical shape using four-stage strategy, the measurement was carried out at 0°, 90°, 180° and 270° positions at various Z-depth by contacting the edge finder at inside of formed surface of the hemisphere. First the edge finder was brought to the position 1 where X and Y position are 0, 0 and Z-depth corresponding to the depth of interest as shown in Figure 13. Then the edge finder is moved to a position 2 where edge finder makes contact with the inside surface of the hemisphere. The corresponding X-positon (distance d) is recorded from the CNC controller. All the measured position of the tool are super-imposed on true profile which is a hemisphere with SR = 29 mm radius using AUTOCAD software. The difference in radial direction e_1 is considered as the geometric error. Table 5 gives a summary of the error for all the positions at different Z-depth. At tool Z-depth of 5 mm geometric error is positive whereas at all other Z-depths it is negative. The reason is that due to bending near the periphery hemisphere is over formed and hence the error is positive. However, after forming due to elastic recovery component springbacks and, hence, the error is negative for other Z-depth values. Maximum profile error comes out to be 0.76 mm which is acceptable for components produced by the SPIF process. At the bottom, error (e_2) in geometry is found to be –0.19 due to springback effect. This error is widely known as Pillow defect in the ISF literature.

It is also observed that stepped feature at the bottom (protrusion defect) is completely eliminated in the formed component using four-stage strategy (Figure 7(d)). It can be attributed to the proper selection of the intermediate stage (part of the hemisphere) and forming the component to a lower depth during the intermediate stage. Hence, protrusion defect can be eliminated without making any calculation of ridig body translation.

Figure 13 Schematic diagram for geometric error measurement

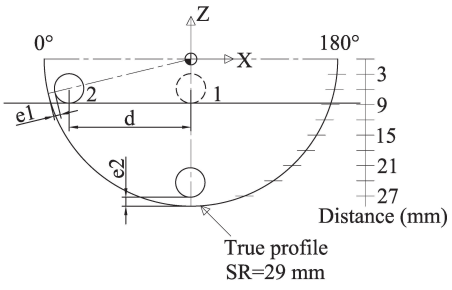

Table 5 Summary of geometric error for component formed using four stage forming strategy

	Position			
Z-depth mm	0° mm	90° mm	180° mm	270° mm
5	0.76	0.38	0.09	0.51
10	–0.01	–0.42	–0.7	–0.32
15	–0.13	–0.49	–0.73	–0.45
20	–0.2	–0.48	–0.67	–0.4
25	–0.1	–0.32	–0.47	–0.3

5.2.2 Thickness distribution

The thickness of the component formed using four-stage forming strategy is measured using pointed anvil micrometer having the least count of 0.001 mm at a regular depth interval of 3 mm. Points were marked on the formed hemisphere using the vernier height gauge as shown in Figure 13. Thickness is measured at 0° position and 180° position by taking three readings which are averaged out to get the confidence and statistical meaning to the measurement. Figure 14 gives the thickness distribution. Hypothetical thickness (t) obtained by volume constancy principle is also shown assuming that a thin circular sheet ($SR = 29$) of uniform thickness (0.71 mm) is converted into the spherical shell ($SR = 29$) of uniform thickness (t). The well known Sine rule is not used for prediction because for the hemispherical shape wall angle varies from 90° (near the base) to 0° (near the pole). From the figure it can be interpreted that thickness at 0° position is less than the thickness at 180° position. This can be attributed to the step-depth which is given at 0° position to form the next contour.

Figure 10 shows the cut section of hemisphere from FE simulation formed using the four-stage forming strategy. From the figure thinning band is visible in-between the depth from 7.017 and 14.892 mm. A similar thinning band is also visible in the formed component and evident from thickness plot (Figure 14). Failure in single-, two- and three-stage strategy always seen in this thinning band.

Thickness history of four elements located at position 1 (A3162, B3549, C3762, D4149) is shown in Figure 15 for a component produced by single-stage and four-stage strategy. It can be seen that for single stage forming strategy maximum thinning occurs for element A3162 and as we move towards D4149 thinning reduces. However, for four-stage strategy, the reverse phenomenon is observed, i.e., element D4149 observes the maximum thinning and the element A3162 observes the minimum thinning. It gives an indication that thinning

band has shifted from the periphery region towards the direction of the pole. Hence, it is confirmed that in four-stage forming strategy, during initial stages, material is deformed in the less stiff area towards pole and less forming in the stiff area near periphery which is the reason for higher formability for four-stage forming strategy.

Figure 14 Measured thickness of component produced by four stage forming strategy (see online version for colours)

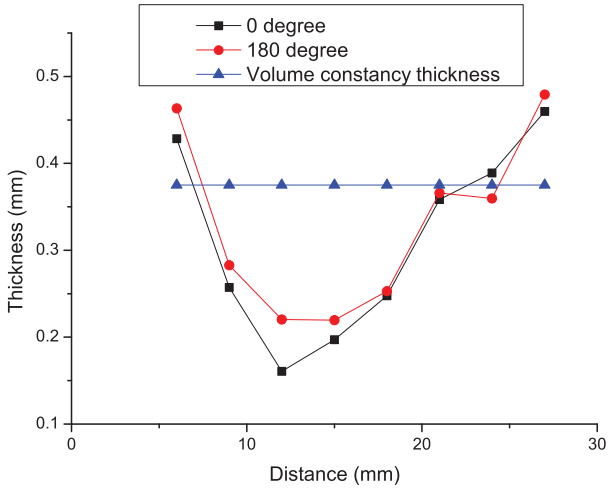

Figure 15 Thickness history of hemispherical component (FEA): (a) single stage and (b) four stage (see online version for colours)

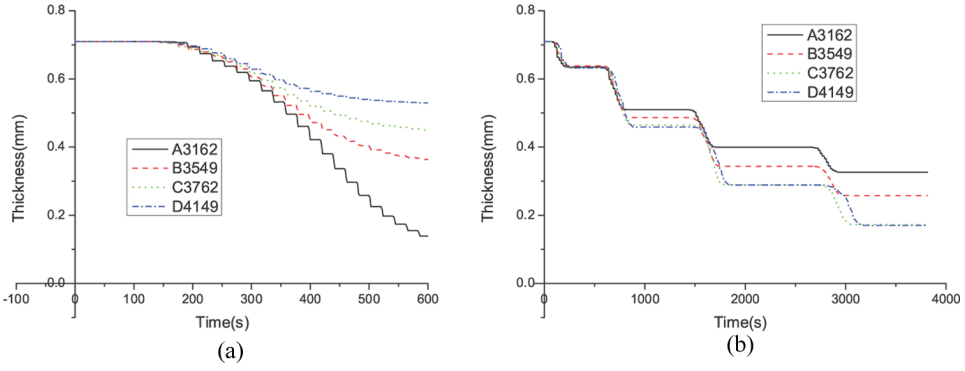

Thickness evolution and thickness strain of element A3162 have been studied for all the strategies and presented in Table 6 and Table 7 respectively. In single-stage streategy high strain of the order of 0.73 is observed by the element A3162 in first-stage. In two-stage strategy thickness strain of 0.33 and 0.61 is observed by the element in first and second stage respectively. First stage is successful, however, component fails in second stage due to high strain. With similar interpretation it is observed that component fails in third stage when three-stage strategy have been used. In four-stage strategy thickness strain is more uniform with the highest value of 0.22 in third stage. It shows that deformation of the

element is gradual and uniform. The result is consistent with the surface area strain analysis presented earlier in which maximum strain of the order of 0.22 for the third stage (Table 4). Thickness evolution and thickness strain of element D4149 is presented in Table 8 and Table 9 respectively. Element A3162 observes higher strains as compared to element D4149 in single stage stragey and hence failure occurs at element A3162. However, strain evolution is more gradual in element D4149 in four stage strategy and hence component is formed successfully.

Table 6 Thickness evolution of element A3162

Strategy	*Initial* mm	*1st stage* mm	*2nd stage* mm	*3rd stage* mm	*4th stage* mm	*Component condition*
Single stage	0.71	0.19				Failure
Two stage	0.71	0.48	0.19			Failure
Three stage	0.71	0.59	0.40	0.27		Failure
Four stage	0.71	0.63	0.51	0.40	0.33	Success

Table 7 Thickness strain evolution of element A3162

Strategy	*1st stage*	*2nd stage*	*3rd stage*	*4th stage*	*Component condition*
Single stage	0.73				Failure
Two stage	0.33	0.61			Failure
Three stage	0.17	0.33	0.31		Failure
Four stage	0.11	0.20	0.22	0.19	Success

Table 8 Thickness evolution of element D4149

Strategy	*Initial* mm	*1st stage* mm	*2nd stage* mm	*3rd stage* mm	*4th stage* mm	*Component condition*
Single stage	0.71	0.47				Failure
Two stage	0.71	0.47	0.30			Failure
Three stage	0.71	0.59	0.33	0.15		Failure
Four stage	0.71	0.63	0.46	0.29	0.17	Success

Table 9 Thickness strain evolution of element D4149

Strategy	*1st stage*	*2nd stage*	*3rd stage*	*4th stage*	*Component condition*
Single stage	0.34				Failure
Two stage	0.34	0.37			Failure
Three stage	0.17	0.44	0.53		Failure
Four stage	0.11	0.27	0.37	0.41	Success

From the FE simulation, % thinning is obtained at the point of failure and summarised in Table. 10. It can be seen that for all the components % thinning is within 79.75±6% value. The von-Mises stress was obtained as 363.45±1% N/mm^2.

Table 10 Percentage thinning and von-Mises stress observed through FE simulation in forming hemispherical component

Strategy	*Thinning* %	*von-Mises stress* N/mm^2
Single stage	78.89	362.0
Two stage	75.62	361.7
Three stage	79.52	366.7
Four stage	84.97	363.4

6 Conclusions

This research was performed to understand the behaviour of sheet metal in multistage forming with special emphasis on multistage tool path strategy as it is one of the important element for the successful forming of the component in the SPIF process. Following conclusions can be drawn based on the experimental and numerical work presented in this paper:

1 Multistage toopath strategy helps to produce the hemispherical component successfully.

2 Moreover, toolpath in every stage is a segment of a sphere, which helps to eliminate the protrusion defect.

3 The limiting value of % increase in surface area for the hemispherical component is of the order of 30. This value can be useful in designing the intermediate stages for hemisphrecal shape. More experimental work is required to find out optimum value of % increase in surface area for other geometrical shapes.

4 Deformation in SPIF process is mainly attributed to meridional strain. However, increase in the number of stages leads to initial biaxial deformation. Though circumferential strain is small, helps to improve formability.

5 Variable step-depth strategy is very much useful in generating shapes like hemisphere with good degree of accuracy. Maximum global accuracy achieved in the current work is of the order of 0.76 mm which is in the bending region near the clamped periphery. It can be improved further by reducing the maximum step-depth to the lower value, however, it will affect the time to produce the component.

6 As number of stages increases tool entry angle decreases which leads to delay in development of thinning band and hence leads to uniform thinning and better formability.

7 The proposed strategy has given a direction to form the component successfully. However, the optimum number of forming stages is to be investigated for various materials. Incrementing the stages as per the limiting value of % increase in surface area (30%) may give minimum number of stages which can be carried out as an extension of the study.

References

Adams, D. and Jeswiet, J. (2015) 'Design rules and applications of single-point incremental forming', *Proceedings of the Institution of Mechanical Engineers, Part B: Journal of Engineering Manufacture*, Vol. 229, No. 5, pp.754–760, https://doi.org/10.1177/0954405414531426

Attanasio, A., Ceretti, E. and Giardini, C. (2006) 'Optimization of tool path in two points incremental forming', *Journal of Materials Processing Technology*, Vol. 177, Nos. 1–3, pp.409–412, https://doi.org/10.1016/j.jmatprotec.2006.04.047

Attanasio, A., Ceretti, E., Giardini, C. and Mazzoni, L. (2008) 'Asymmetric two points incremental forming: improving surface quality and geometric accuracy by tool path optimization', *Journal of Materials Processing Technology*, Vol. 197, Nos. 1–3, pp.59–67, https://doi.org/10.1016/j.jmatprotec.2007.05.053

Bambach, M., Araghi, B.T. and Hirt, G. (2009) 'Strategies to improve the geometric accuracy in asymmetric single point incremental forming', *Production Engineering*, Vol. 3, No. 2, pp.145–156, https://doi.org/10.1007/s11740-009-0150-8

Behera, A.K., Lauwers, B. and Duflou, J.R. (2014) 'Tool path generation framework for accurate manufacture of complex 3D sheet metal parts using single point incremental forming', *Computers in Industry*, Vol. 65, No. 4, pp.563–584, https://doi.org/10.1016/j.compind.2014.01.002

Bouhamed, A., Jrad, H., Said, L.B., Wali, M. and Dammak, F. (2019a) 'A non-associated anisotropic plasticity model with mixed isotropickinematic hardening for finite element simulation of incremental sheet metal forming process', *The International Journal of Advanced Manufacturing Technology*, Vol. 100, Nos. 1–4, pp.929–940, https://doi.org/10.1007/s00170- 018-2782-3

Bouhamed, A., Jrad, H., Mars, J., Wali, M., Gamaoun, F. and Dammak, F. (2019b) 'Homogenization of elasto-plastic functionally graded material based on representative volume element: application to incremental forming process', *International Journal of Mechanical Sciences*, Vol. 160, pp.412–420, https://doi.org/10.1016/j.ijmecsci.2019.07.005

Centeno, G., Silva, M.B., Cristino, V.A.M., Vallellano, C. and Martins, P.A.F. (2012) 'Hole-flanging by incremental sheet forming', *International Journal of Machine Tools and Manufacture*, Vol. 59, pp.46–54, https://doi.org/10.1016/j.ijmachtools.2012.03.007

Cui, Z. and Gao, L. (2010) 'Studies on hole-flanging process using multistage incremental forming', *CIRP Journal of Manufacturing Science and Technology*, Vol. 2, No. 2, pp.124–128, https://doi.org/10.1016/j.cirpj.2010.02.001.

Dai, K., Wang, Z.R. and Fang, Y. (2000) 'CNC incremental sheet forming of an axially symmetric specimen and the locus of optimization', *Journal of Materials Processing Technology*, Vol. 102, Nos. 1–3, pp.164–167, https://doi.org/10.1016/S0924-0136(00)00423-4

Duflou, J.R., Verbert, J., Belkassem, B., Gu, J., Sol, H., Henrard, C. and Habraken, A.M. (2008) 'Process window enhancement for single point incremental forming through multi-step toolpaths', *CIRP Annals*, Vol. 57, No. 1, pp.253–256, https://doi.org/10.1016/j.cirp.2008.03.030

Fiorentino, A., Marzi, R. and Ceretti, E. (2012) 'Preliminary results on Ti incremental sheet forming (ISF) of biomedical devices: biocompatibility, surface finishing and treatment', *International Journal of Mechatronics and Manufacturing Systems*, Vol. 5, No. 1, pp.36–45, https://doi.org/10.1504/IJMMS.2012.046146

Giraldo-Castrillon, F.A., Giraldo-Castrillon, Y.M. and Páramo-Bermúdez, G.J. (2019) 'Statistical analysis of the parameters in SPIF/DPIF in the thickness reduction in an experimental geometry', *International Journal of Mechatronics and Manufacturing Systems*, Vol. 12, No. 2, pp.96–115, https://doi.org/10.1504/IJMMS.2019.102946

Jackson, K. and Allwood, J. (2009) 'The mechanics of incremental sheet forming', *Journal of Materials Processing Technology*, Vol. 209, No. 3, pp.1158–1174, https://doi.org/10.1016/j.jmatprotec.2008.03.025

Kim, T.J. and Yang, D.Y. (2000) 'Improvement of formability for the incremental sheet metal forming process', *International Journal of Mechanical Sciences*, Vol. 42, No. 7, pp.1271–1286, https://doi.org/10.1016/S0020-7403(99)00047-8

Li, Y., Chen, X., Liu, Z., Sun, J., Li, F., Li, J. and Zhao, G. (2017) 'A review on the recent development of incremental sheet-forming process', *The International Journal of Advanced Manufacturing Technology*, Vol. 92, Nos. 5–8, pp.2439–2462, https://doi.org/10.1007/s00170-017-0251-z

Liu, Z., Daniel, W.J., Li, Y., Liu, S. and Meehan, P.A. (2014) 'Multi-pass deformation design for incremental sheet forming: analytical modeling, finite element analysis and experimental validation', *Journal of Materials Processing Technology*, Vol. 214, No. 3, pp.620–634, https://doi.org/10.1016/j.jmatprotec.2013.11.010

LSTC (2015) *LS-DYNA Keyword User's Manual*, Vols. 1–3.

Lu, B., Chen, J., Ou, H. and Cao, J. (2013) 'Feature-based tool path generation approach for incremental sheet forming process', *Journal of Materials Processing Technology*, Vol. 213, No. 7, pp.1221–1233, https://doi.org/10.1016/j.jmatprotec.2013.01.023

Malhotra, R., Reddy, N.V. and Cao, J. (2010) 'Automatic 3D spiral toolpath generation for single point incremental forming', *Journal of Manufacturing Science and Engineering*, Vol., 132, No. 6, p.061003-1-10, https://doi.org/10.1115/1.4002544

Malhotra, R., Bhattacharya, A., Kumar, A., Reddy, N.V. and Cao, J. (2011) 'A new methodology for multi-pass single point incremental forming with mixed toolpaths', *CIRP Annals*, Vol. 60, No. 1, pp.323–326, https://doi.org/10.1016/j.cirp.2011.03.145

Malhotra, R., Cao, J., Beltran, M., Xu, D., Magargee, J., Kiridena, V. and Xia, Z.C. (2012) 'Accumulative-DSIF strategy for enhancing process capabilities in incremental forming', *CIRP Annals*, Vol. 61, No. 1, pp.251–254, https://doi.org/10.1016/j.cirp.2012.03.093

Manco, L., Filice, L. and Ambrogio, G. (2011) 'Analysis of the thickness distribution varying tool trajectory in single-point incremental forming', *Proceedings of the Institution of Mechanical Engineers, Part B: Journal of Engineering Manufacture*, Vol. 225, No. 3, pp.348–356, https://doi.org/10.1177/09544054JEM1958

Smith, J., Malhotra, R., Liu, W.K. and Cao, J. (2013) 'Deformation mechanics in single-point and accumulative double-sided incremental forming', *The International Journal of Advanced Manufacturing Technology*, Vol. 69, Nos. 5–8, pp.1185–1201, https://doi.org/10.1007/s00170-013-5053-3

Xu, D., Malhotra, R., Reddy, N.V., Chen, J. and Cao, J. (2012) 'Analytical prediction of stepped feature generation in multi-pass single point incremental forming', *Journal of Manufacturing Processes*, Vol. 14, No. 4, pp.487–494, https://doi.org/10.1016/j.jmapro.2012.08.003